Strontium doping effect on phase homogeneity and conductivity of Ba1−xSrxCe0.6Zr0.2Y0.2O3− proton-conducting oxides

ARTICLE *in* INTERNATIONAL JOURNAL OF HYDROGEN ENERGY · AUGUST 2013

Impact Factor: 3.31 · DOI: 10.1016/j.ijhydene.2013.01.043

Available online at www.sciencedirect.com

SciVerse ScienceDirect

journal homepage: www.elsevier.com/locate/he

Strontium doping effect on phase homogeneity and conductivity of $Ba_{1-x}Sr_xCe_{0.6}Zr_{0.2}Y_{0.2}O_{3-\delta}$ proton-conducting oxides

Kan-Rong Lee [a,b], Chung-Jen Tseng [b], Jeng-Kuei Chang [a], I-Ming Hung [c], Jing-Chie Lin [a], Sheng-Wei Lee [a,*]

[a] Institute of Materials Science and Engineering, National Central University, No. 300, Jhongda Road, Jhongli City, 32001 Taiwan, ROC

[b] Department of Mechanical Engineering, National Central University, Jhongli City, 32001 Taiwan, ROC

[c] Department of Chemical Engineering and Materials Science, Yuan Ze University, Jhongli City, 32003 Taiwan, ROC

ARTICLE INFO

Article history:
Received 28 October 2012
Received in revised form
14 December 2012
Accepted 1 January 2013
Available online 6 February 2013

Keywords:
Proton-conducting electrolyte
Solid oxide fuel cells
$Ba_{1-x}Sr_xCe_{0.6}Zr_{0.2}Y_{0.2}O_{3-\delta}$
Chemical stability
Ionic conductivity

ABSTRACT

$Ba_{1-x}Sr_xCe_{0.6}Zr_{0.2}Y_{0.2}O_{3-\delta}$ ($0.0 \leq x \leq 1.0$) proton-conducting oxides have been prepared using a citrate-EDTA complexing sol–gel method. In this study, the relationship between the Sr doping content and microstructure, chemical stability against CO_2, and conductivity of the sintered $Ba_{1-x}Sr_xCe_{0.6}Zr_{0.2}Y_{0.2}O_{3-\delta}$ pallets are systematically investigated using XRD, SEM, micro-Raman spectroscopy, and dc two-probe measurements. All sintered $Ba_{1-x}Sr_xCe_{0.6}Zr_{0.2}Y_{0.2}O_{3-\delta}$ oxides exhibit excellent chemical stability after being exposed to the CO_2 ambient at 600 °C for a long duration; nevertheless, their microstructures and conductivities are very sensitive to the Sr doping amount. The Sr incorporation is found to apparently suppress the formation of CeO_2-like second phase, and enhance the grain growth in sintered oxides. Among all sintered samples, the $Ba_{0.8}Sr_{0.2}Ce_{0.6}Zr_{0.2}Y_{0.2}O_{3-\delta}$ pallet has the highest conductivity, 0.009 S/cm at 800 °C. This result can be attributed to the competition between the elimination of CeO_2- or $(Zr,Ce,Y)O_2$-like phase inhomogeneity and enhanced grain growth in sintered oxides, both of which adversely influence the ionic conductivity. This work demonstrates that $Ba_{1-x}Sr_xCe_{0.6}Zr_{0.2}Y_{0.2}O_{3-\delta}$ would be a promising electrolyte for H^+-SOFC applications if the Sr doping is well controlled.

1. Introduction

During the past decades, solid oxide fuel cells (SOFCs) have attracted considerable attention as promising power-generation systems due to their high thermodynamic efficiency, low environmental impact, fuel flexibility, and ability to use non-precious-metal catalysts [1–3]. Traditional SOFCs composed of oxygen-ion-conducting electrolytes usually require operation at a temperature of approximately 1000 °C. However, such a high operation temperature can lead to many practical problems, such as high costs, materials degradations, reactions between the components, and a long start-up and shut-off period [4,5], etc. Therefore, there has been great interest in SOFCs based on proton-conducting electrolytes (H^+-SOFCs) operating at an intermediate temperature range of 400–800 °C that facilitates the selection of the sealing and

* *Corresponding author*. Tel.: +886 3 4227151x34905; fax: +886 3 2805034.
E-mail address: schon0911@gmail.com (S.-W. Lee).

0360-3199/$ – see front matter
http://dx.doi.org/10.1016/j.ijhydene.2013.01.043

interconnection materials, control of the interactions between the electrode/electrolyte, and prolongs the operational lifetime [6–8]. The key issue in the development of H^+-SOFC is the use of a highly proton-conductive electrolyte with stable structure at intermediate temperatures.

Perovskite-type oxides such as $BaCeO_3$, $BaZrO_3$, $SrCeO_3$, and $SrZrO_3$ doped with rare-earth elements are known to be protonic conductors [9]. Iwahara et al. demonstrated that $BaCeO_3$ has the highest protonic conductivity among these conductors [10,11]. Several synthesis techniques have been utilized to fabricate $BaCeO_3$-based powders, including solid-state reaction [12], hydrothermal reaction [13], combustion [14] and sol–gel [15]. The sol–gel process has attracted great interest because it can produce powders with great compositional uniformity, low residual carbon level, and nano-scale particle size [16,17], which is important to make dense products at lower sintering temperatures. In addition, the resulting nano-crystalline conductors have been reported to have the higher conductivity compared to micro-scale oxides prepared using other processes due to favorable ionic mobility along the grain boundaries [18]. Besides the synthesis method, it is believed that the type and ratio of the dopants also strongly influence their electrical properties. To enhance the protonic conduction in $BaCeO_3$, doping with lower-valence cations, as well as introducing water vapor, is essential. A trivalent dopant such as Y^{3+} can lead to the creation of oxygen vacancies, thus resulting in enhanced protonic conduction.

Another challenging issue in Y-doped $BaCeO_3$ electrolytes for H^+-SOFC applications is thermal instability due to the reaction with CO_2-, H_2O-, or H_2S-containing atmospheres [19–21]. Such unfavorable reactions with carbon species and H_2S could cause performance loss and degradation. Partially substituting Zr for Ce can reduce tendency of decomposition in CO_2 at high temperature but also decreases the ionic conductivity [17]. Fabbri et al. has reported the promising performance observed for $BaCe_{0.3}Zr_{0.5}Y_{0.2}O_{3-\delta}$ since it maintained the good chemical stability of barium zirconate but with improved fuel cell performance [22]. Thermodynamically, the chemical stability of $SrCeO_3$ is also higher than that of $BaCeO_3$ [23]. Accordingly, this study designs and synthesizes $Ba_{1-x}Sr_xCe_{0.6}Zr_{0.2}Y_{0.2}O_{3-\delta}$ ($0.0 \le x \le 1.0$) oxides by using citrate-ethylenediaminetetraacetic acid (EDTA) complexing sol–gel method. The aim of the present study is to clarify the relationship between the Sr doping content and microstructure, chemical stability against CO_2, and conductivity of Y-doped Ba–Sr mixed perovskite proton-conducting oxides.

2. Experimental

The citrate-EDTA complexing sol–gel process is used for preparing $Ba_{1-x}Sr_xCe_{0.6}Zr_{0.2}Y_{0.2}O_{3-\delta}$ ($0.0 \le x \le 1.0$) oxides. The starting materials were commercial $Ba(NO_3)_2$ (J. T.Baker, 99.3%), $Sr(NO_3)_2$ (Alfa Aesar, 99.0%), $ZrO(NO_3)_2{\cdot}2H_2O$ (Showa, 99.0%), $Ce(NO_3)_3{\cdot}6H_2O$ (Alfa Aesar, 99.5%), and $Y(NO_3)_3{\cdot}6H_2O$ (Alfa Aesar, 99.9%). Both citric acid and EDTA were used as chelating agents to the precursor solution. The molar ratio of citric acid and EDTA to the total metal cations content was set at 2:2:3. The pH value of the solution was adjusted to be around 6 using NH_4OH. The mixed solutions were heated to 100 °C under stirring until obtaining viscous gels. By further heated at 250 °C to evaporate residual water and organics, these gels were converted into black powders. The synthesized powders were then calcined at 1000 °C for 12 h with a heating rate of 5 °C/min. To obtain dense samples, the calcined powders were uniaxially pressed into cylindrical pellets (1 cm in diameter and 1 mm in thickness) at 250 MPa for 20 s and then sintered in an air atmosphere. Sintering was carried out at 1600 °C for 4 h. The chemical stability of $Ba_{1-x}Sr_xCe_{0.6}Zr_{0.2}Y_{0.2}O_{3-\delta}$ oxides was evaluated by exposing the sintered pellets to the CO_2 ambient (99.99%) at 600 °C for 16 h.

The phase identification of the sintered oxides was performed with a powder diffractometer (Bruker D8A) with Ni-filtered Cu K_α radiation and the diffraction angle from 20° to 80° with a step of 0.01°. Morphologies of the sintered pallets were examined using field-emission scanning electron microscope (FESEM, FEI NOVA 230) in conjunction with an energy dispersion spectrometer (EDS). The conductivities of the sintered pellets were measured by a dc two-probe method; the measurements were performed in air with 3% relative humidity in the temperature range of 400 ~ 800 °C. Silver ink was painted on both faces of the pellets to create current collectors and the measurement data were acquired using an Agilent 34970A meter. In order to study the local configuration of chemical bonding in $Ba_{1-x}Sr_xCe_{0.6}Zr_{0.2}Y_{0.2}O_{3-\delta}$ oxides, Raman spectra were acquired using an Andor SR-500i spectrometer with a spectral resolution of 0.5 cm^{-1}. The Raman spectra were excited by a diode-pumped solid-state (DPSS) laser line with wavelength of 532 nm in a near-backscattering geometry. Raman signal mapping was also performed within a 100 μm × 100 μm area on the sintered pellets with a spatial resolution of 1 μm.

3. Results and discussion

As shown in Fig. 1a, all sintered $Ba_{1-x}Sr_xCe_{0.6}Zr_{0.2}Y_{0.2}O_{3-\delta}$ oxides are predominantly the perovskite-type cubic structure, showing five major diffraction signals, namely those from the (110), (200), (211), (220), and (310) planes (JCPDS card no. 89-2485). To further verify the formation of the solid solution over the whole range of Sr doping content ($0.0 \le x \le 1.0$), the lattice constants were determined from XRD analysis based on cubic lattice symmetry and the results as shown in Fig. 1b. A nearly linear relation between lattice parameter and Sr doping content is observed. Such a phenomenon can be well explained by the fact that Sr^{2+} (1.18 Å) has a smaller ionic radius than Ba^{2+} (1.35 Å) at the A-site of perovskite structure [24]. In addition, four weak broad peaks associated with the cubic $(Zr,Ce,Y)O_2$-like structure indicated by "▲" are observed in Fig. 1a [25]. These peaks most likely correspond to a CeO_2-like phase since their XRD peaks close to main peaks of CeO_2. As the Sr doping content increases, these CeO_2-like peaks gradually vanish, indicating that the Sr incorporation can suppress the formation of CeO_2-like second phase in $Ba_{1-x}Sr_xCe_{0.6}Zr_{0.2}Y_{0.2}O_{3-\delta}$ oxides. We speculate that the smaller Sr^{2+} at the A-site of

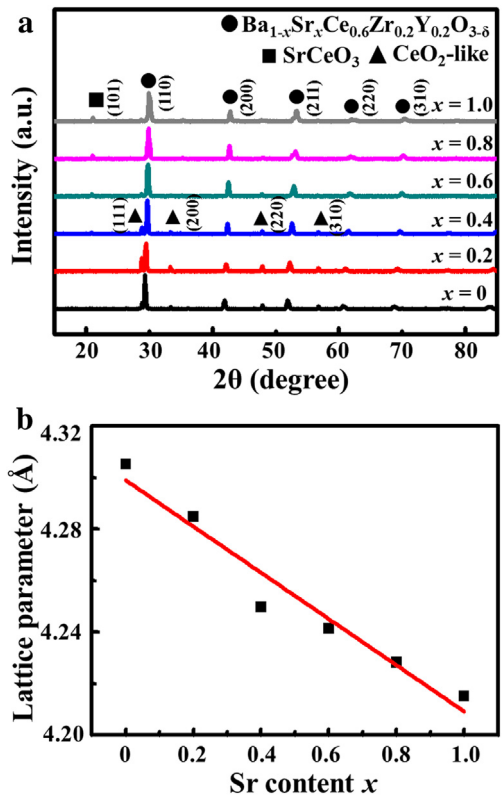

Fig. 1 – (a) XRD patterns of the synthesized $Ba_{1-x}Sr_xCe_{0.6}Zr_{0.2}Y_{0.2}O_{3-\delta}$ ($0.0 \le x \le 1.0$) oxides with various Sr contents after sintering at 1600 °C for 4 h, (b) lattice constants of $Ba_{1-x}Sr_xCe_{0.6}Zr_{0.2}Y_{0.2}O_{3-\delta}$ oxides as a function of Sr contents based on cubic lattice symmetry.

perovskites may be beneficial for the volume compensation balanced by the larger Ce^{4+} ion (0.87 Å, and Zr^{4+} ~ 0.72 Å) at the B-site [25], and thus facilitate the Ce incorporation into perovskites and retard the precipitation of CeO_2-like phase. Nevertheless, another second phase, $SrCeO_3$, starts to appear as the Sr doping content exceeds 0.6.

Fig. 2a–f show the surface morphologies of the sintered $Ba_{1-x}Sr_xCe_{0.6}Zr_{0.2}Y_{0.2}O_{3-\delta}$ ($0.0 \le x \le 1.0$) pellets. Generally, these ceramic pellets are well densified, and very few pores are observed on the pellet surface. The pores can be ascribed to the oxide volume shrinkage that resulted from the release of structural water and residual organics during high-temperature treatment. Fig. 2g shows a typical SEM micrograph taken from the fractured cross section of a sintered pellet ($Ba_{0.8}Sr_{0.2}Ce_{0.6}Zr_{0.2}Y_{0.2}O_{3-\delta}$). The image indicates that the interior oxide is also well densified (i.e., the open pores are only on the surface), indicating the great sinterability of the oxide powders synthesized by sol–gel. Although a few enclosed voids are observed, they are not connected throughout the sintered oxide. This compact ceramic layer (not fuel-permeable) can be a suitable electrolyte for the use in H^+-SOFCs. In addition, the Sr incorporation apparently influences the grain size of the sintered oxides. Both $BaCe_{0.6}Zr_{0.2}Y_{0.2}O_{3-\delta}$ and $Ba_{0.8}Sr_{0.2}Ce_{0.6}Zr_{0.2}Y_{0.2}O_{3-\delta}$ (Fig. 2a and b) show a small grain size feature, nevertheless, the grain size noticeably increases once the Sr doping content is further increased ≥0.4. Moreover, the $SrCe_{0.6}Zr_{0.2}Y_{0.2}O_{3-\delta}$ pellet (see Fig. 2f) reveals a few small inclusions (typically ~1–3 μm in size) located predominantly in grain boundary regions. EDS analysis confirms enrichment in Sr and Ce and depletion of Ba in these inclusions (see Fig. 2h), suggesting that they may correspond to the $SrCeO_3$ second phase as previously identified by XRD.

One advantage of H^+-SOFCs over low-temperature polymer-electrolyte fuel cells (PEFC) is the capable of using hydrocarbon fuels (instead of pure hydrogen) [26]. The hydrocarbon gas can be in-situ reformed into CO_2 and H_2 by the catalysts on the H^+-SOFC anodes. Therefore, the operational reliability of oxide electrolytes in the CO_2- or H_2O-containing atmosphere is essential. In order to verify the chemical stability of our prepared oxides, the sintered $Ba_{1-x}Sr_xCe_{0.6}Zr_{0.2}Y_{0.2}O_{3-\delta}$ pellets were exposed to pure CO_2 in a tube furnace at 600 °C for long durations and the phase evolution was investigated by XRD. All sintered $Ba_{1-x}Sr_xCe_{0.6}Zr_{0.2}Y_{0.2}O_{3-\delta}$ pellets exhibit excellent chemical stability against CO_2 even after exposure to CO_2 for 16 h Fig. 3 shows the representative results for the $Ba_{1-x}Sr_xCe_{0.6}Zr_{0.2}Y_{0.2}O_{3-\delta}$ pellets with two extreme Sr compositions: $x_{Sr} = 0$ and 1.0. The XRD peaks from original phase remain almost unchanged and no obvious decomposition of the perovskite phase is detected. Guo et al. [17] studied the chemical stability of proton-conducting $BaZr_yCe_{0.8-y}Y_{0.2}O_{3-\delta}$, indicating that if $y < 0.4$, the perovskite structure is destroyed in a CO_2 atmosphere at 650 °C for 2 h. The sintered $Ba_{1-x}Sr_xCe_{0.6}Zr_{0.2}Y_{0.2}O_{3-\delta}$ electrolytes in the present study should possess sufficient reliability in the H^+-SOFC operation environment.

Electrolyte conduction also greatly affects the overall energy conversion performance of H^+-SOFCs. Here, the ionic conductivities of the $Ba_{1-x}Sr_xCe_{0.6}Zr_{0.2}Y_{0.2}O_{3-\delta}$ oxides are evaluated as a function of temperatures in an air atmosphere with 3% relative humidity. Fig. 4 summarizes the measurement data. The increase in conductivity with increasing temperature indicates that the $Ba_{1-x}Sr_xCe_{0.6}Zr_{0.2}Y_{0.2}O_{3-\delta}$ oxides exhibit ionic conduction. However, there exists an unusual relation between the Sr content and ionic conductivity. Compared to the $BaCe_{0.6}Zr_{0.2}Y_{0.2}O_{3-\delta}$ ($x_{Sr} = 0$) sample, the conductivity is apparently enhanced by incorporating Sr with the content of 0.2. Among all sintered pallets at 800 °C, the $Ba_{0.8}Sr_{0.2}Ce_{0.8}Zr_{0.2}Y_{0.2}O_{3-\delta}$ conductor has the highest conductivity as high as 0.009 S/cm. This value is lower than that of the $BaCe_{0.45}Zr_{0.45}Y_{0.1}O_{3-\delta}$ oxide (~0.0106 S/cm) [27], but is comparable to those of In-, Gd-, Sm-, Sc-, and Nd-doped $BaCeO_3$-based electrolytes at the same temperature of 800 °C (In-doped: 0.005 S/cm, Gd-doped: 0.0082 S/cm, Sm-doped: 0.0069 S/cm, Sc-doped: 0.0027 S/cm, Nd-doped: 0.00298 S/cm at 700 °C) [27–29]. It is expected that this value can be further improved by tuning the experimental parameters. Nevertheless, increasing the Sr doping content to 0.4–0.6 slightly decreases the conductivity. Further increasing the Sr doping to the content ≥0.8 dramatically decreases the oxide conductivity. It has been proposed that the ionic conductivity at grain boundaries is higher than that in the bulk oxide [5,18]. According to the above-mentioned results, the Sr content ≥0.4 can apparently enhance the grain growth or even precipitate $SrCeO_3$ in $Ba_{1-x}Sr_xCe_{0.6}Zr_{0.2}Y_{0.2}O_{3-\delta}$ oxides. Therefore, it is understandable that increasing the

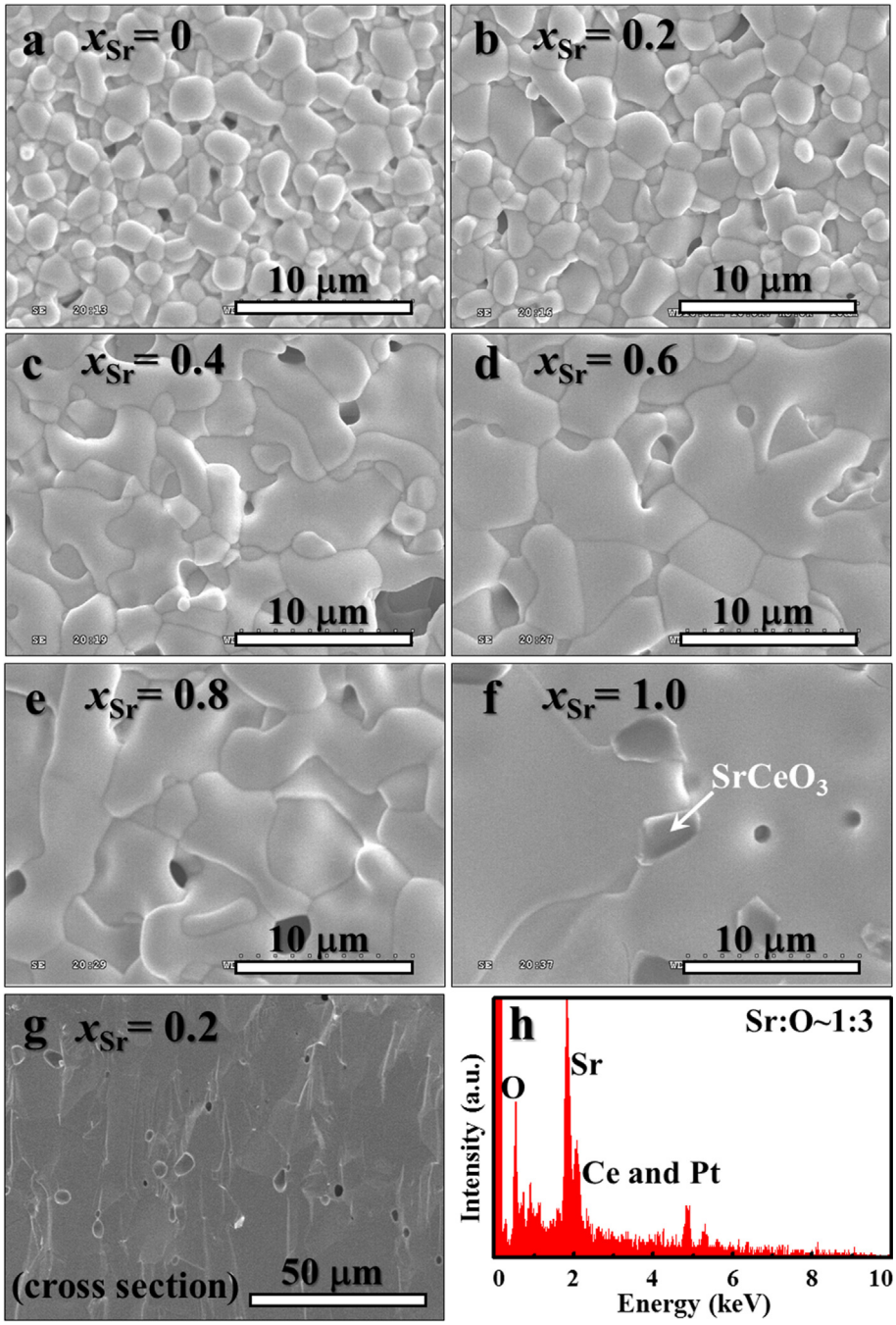

Fig. 2 – FESEM micrographs of surface morphologies of the $Ba_{1-x}Sr_xCe_{0.6}Zr_{0.2}Y_{0.2}O_{3-\delta}$ pellets with (a) $x = 0$, (b) $x = 0.2$, (c) $x = 0.4$, (d) $x = 0.6$, (e) $x = 0.8$, and (f) $x = 1.0$. (g) Fractured cross-section view of the sintered $Ba_{0.8}Sr_{0.2}Ce_{0.6}Zr_{0.2}Y_{0.2}O_{3-\delta}$ pellet. (h) EDS spectrum corresponds to the $SrCeO_3$ grain indicated in (f). Note that Pt signal came from the Pt coating for SEM observation.

Sr doping amount decreases the ionic conductivity. What then is the cause of the enhanced conductivity observed in the $Ba_{0.8}Sr_{0.2}Ce_{0.8}Zr_{0.2}Y_{0.2}O_{3-\delta}$ pallet? We speculate that elimination of CeO_2-like or $(Zr,Ce,Y)O_2$-like second phase may play an important role in this enhancement. This inference can be further verified by the Raman measurements.

Raman spectroscopy was utilized to study the local configuration of chemical bonding in the $Ba_{1-x}Sr_xCe_{0.6}Zr_{0.2}Y_{0.2}O_{3-\delta}$ oxides in this study. Fig. 5 shows the representative Raman spectra of all sintered pallets. Several Raman-active modes, such as ZrO_2-like, CeO_2-like, and Y_2O_3-like phonon vibrations, have been reported for $Ba(Zr_{0.8-x}Ce_xY_{0.2})O_{3-\delta}$ perovskites [30]. The broad Raman peak around 480 cm^{-1} most likely corresponds to the $(Ce,Zr)O_2$-like structures, since the major Raman peaks of CeO_2 and ZrO_2 powders locate at 461 and 474 cm^{-1}, respectively [31,32]. A weak broaden peak around 750 cm^{-1}

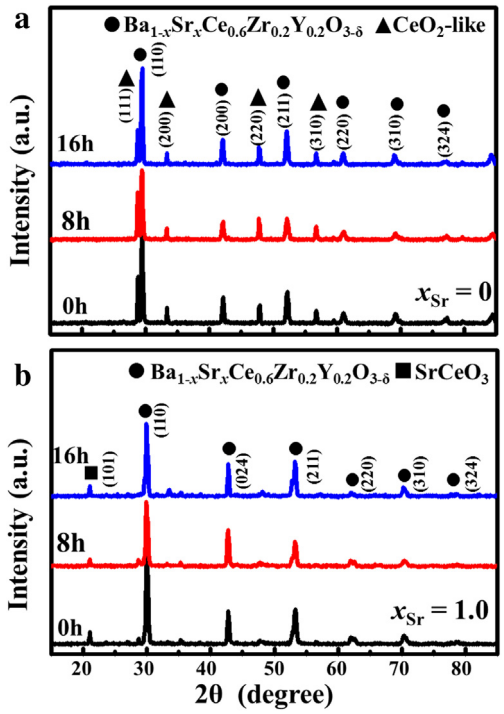

Fig. 3 – XRD patterns of the sintered $Ba_{1-x}Sr_xCe_{0.6}Zr_{0.2}Y_{0.2}O_{3-\delta}$ oxides with the Sr composition of (a) $BaCe_{0.6}Zr_{0.2}Y_{0.2}O_{3-\delta}$ and (b) $SrCe_{0.6}Zr_{0.2}Y_{0.2}O_{3-\delta}$ after exposure to a CO_2 atmosphere at 600 °C for 8 h and 16 h.

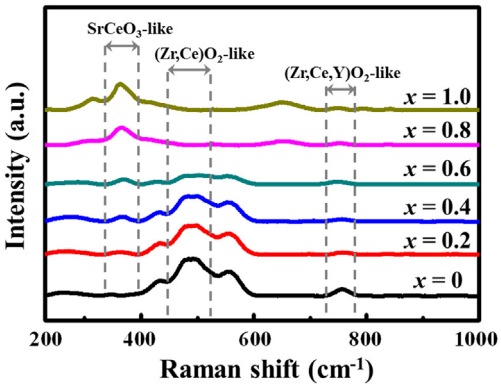

Fig. 5 – Raman spectra of the sintered $Ba_{1-x}Sr_xCe_{0.6}Zr_{0.2}Y_{0.2}O_{3-\delta}$ ($0.0 \le x \le 1.0$) oxides with various Sr contents.

associated with the $(Ce,Zr,Y)O_2$-like second phase is also observed [30]. As the Sr doping content increases, these vibrations slightly shift toward higher frequencies due to the reduction of effective atomic mass and its relative intensity decreases as well. It is consistent with the XRD results that CeO_2-like phase gradually vanishes with the Sr incorporation. The Raman intensity of the $(Ce,Zr,Y)O_2$-like band at 750 cm^{-1} is mapped over the $BaCe_{0.6}Zr_{0.2}Y_{0.2}O_{3-\delta}$ and $Ba_{0.8}Sr_{0.2}Ce_{0.6}Zr_{0.2}Y_{0.2}O_{3-\delta}$ pallets, respectively, as shown in Fig. 6. It is evident that $BaZr_{0.2}Ce_{0.6}Y_{0.2}O_{3-\delta}$ reveals a non-uniform distribution of $(Ce,Zr,Y)O_2$-like second phase in the mapping region. On the contrary, for the $Ba_{0.8}Sr_{0.2}Ce_{0.6}Zr_{0.2}Y_{0.2}O_{3-\delta}$ sample, the measured signal intensity is much weaker and almost identical to the background level, indicating high phase homogeneity of the sintered pallet. This may well explain why the $Ba_{0.8}Sr_{0.2}Ce_{0.6}Zr_{0.2}Y_{0.2}O_{3-\delta}$ pallet has the highest conductivity among all sintered pallets, which is a result of the competition between the elimination of CeO_2- or $(Ce,Zr,Y)O_2$-like phase inhomogeneity and enhanced grain

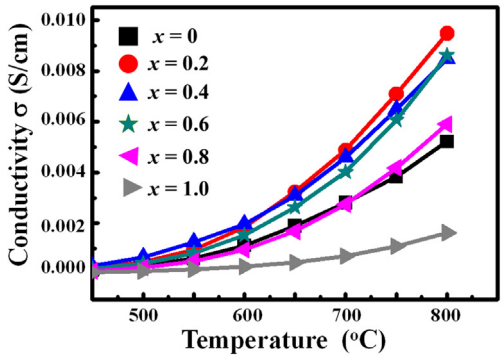

Fig. 4 – Conductivities of the sintered $Ba_{1-x}Sr_xCe_{0.6}Zr_{0.2}Y_{0.2}O_{3-\delta}$ pellets with various Sr contents as a function of testing temperature.

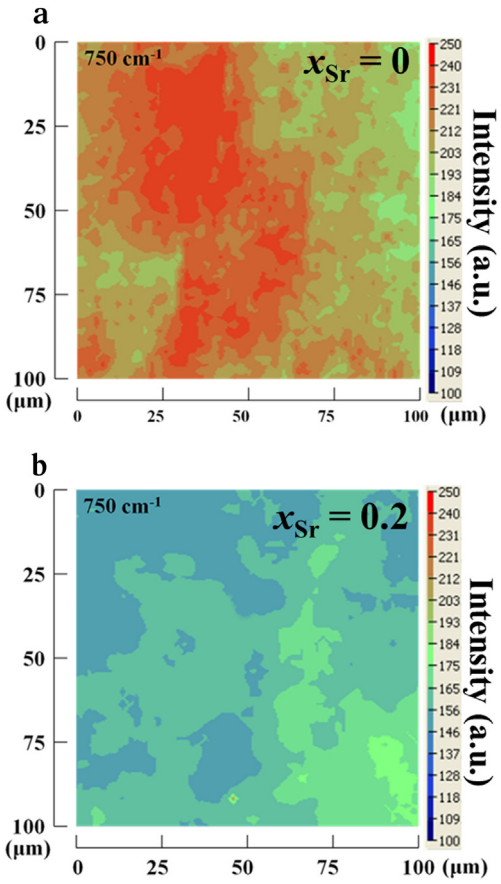

Fig. 6 – Raman mapping of the $(Zr,Ce,Y)O_2$-like band at 750 cm^{-1} on the sintered (a) $BaCe_{0.6}Zr_{0.2}Y_{0.2}O_{3-\delta}$ and (b) $Ba_{0.8}Sr_{0.2}Ce_{0.6}Zr_{0.2}Y_{0.2}O_{3-\delta}$ pallets, respectively.

growth in sintered oxides, both of which adversely influence the conductivity.

4. Conclusions

This study has systematically investigated the relationship between the Sr doping content and microstructure, chemical stability, and conductivity of $Ba_{1-x}Sr_xCe_{0.6}Zr_{0.2}Y_{0.2}O_{3-\delta}$ oxides prepared by a sol–gel method. All sintered $Ba_{1-x}Sr_xCe_{0.6}Zr_{0.2}Y_{0.2}O_{3-\delta}$ pallets exhibit excellent chemical stability against CO_2; nevertheless, their microstructural and electrical properties are very sensitive to the Sr doping content. The Sr incorporation is found to apparently suppress the formation of CeO_2-like second phase, and enhance the grain growth in the sintered oxides. Among all sintered samples, the $Ba_{0.8}Sr_{0.2}Ce_{0.6}Zr_{0.2}Y_{0.2}O_{3-\delta}$ pallet has the highest conductivity as high as 0.009 S/cm at 800 °C. This result can be ascribed to the competition between the elimination of CeO_2- or (Zr,Ce,Y)O_2-like phase inhomogeneity and enhanced grain growth in sintered oxides, both of which adversely influence the ionic conductivity. This study shows that $Ba_{1-x}Sr_xCe_{0.6}Zr_{0.2}Y_{0.2}O_{3-\delta}$ oxides would be a promising electrolyte for the use in H^+-SOFCs if the Sr doping is well controlled.

Acknowledgments

The research is supported by National Nano Device Laboratories and National Science Council of Taiwan under Contracts No. NSC 101-3113-P-008-006 and NSC 100-2221-E- 008-016-MY3. The authors also thank National Nano Device Laboratories and Center for Nano Science and Technology at National Central University for the facility support.

REFERENCES

[1] Murray EP, Tsai T, Barnett SA. A direct-methane fuel cell with a ceria-based anode. Nature 1999;400:649–51.
[2] Chan SH, Ho HK, Tian Y. Multi-level modeling of SOFC-gas turbine hybrid system. Int J Hydrogen Energy 2003;28: 889–900.
[3] Haile SM. Fuel cell materials and components. Acta Mater 2003;51:5981–6000.
[4] Xie K, Yanb RQ, Liua XQ. Stable $BaCe_{0.7}Ti_{0.1}Y_{0.2}O_{3-\delta}$ proton conductor for solid oxide fuel cells. J Alloys Compd 2009;479: 40–2.
[5] Hung IM, Peng HW, Zheng SL, Lin CP, Wu JS. Phase stability and conductivity of $Ba_{1-y}Sr_yCe_{1-x}Y_xO_{3-\delta}$ solid oxide fuel cell electrolyte. J Power Sources 2009;193:155–9.
[6] Shao ZP, Haile SM. A high-performance cathode for the next generation of solid-oxide fuel cells. Nature 2004;431:170–3.
[7] Yang L, Zuo CD, Wang SH, Cheng Z, Liu M. A novel composite cathode for low-temperature SOFCs based on oxide proton conductors. Adv Mater 2008;20:3280–3.
[8] Tan WY, Zhong Q, Miao MS, Qu HX. H_2S Solid oxide fuel cell based on a modified barium cerate perovskite proton conductor. Ionics 2009;15:385–8.
[9] Lin Y, Ran R, Zheng Y, Shao ZP, Jin WQ, Xu NP, et al. Evaluation of $Ba_{0.5}Sr_{0.5}Co_{0.8}Fe_{0.2}O_{3-\delta}$ as a potential cathode for an anode-supported proton- conducting solid-oxide fuel cell. J Power Sources 2008;180:15–22.
[10] Iwahara H, Uchida H, Ono K, Ogaki K. Proton conduction in sintered oxides based on $BaCeO_3$. J Electrochem Soc 1988;135: 529–33.
[11] Iwahara H. Technological challenges in the application of proton conducting ceramics. Solid State Ionics 1995;77: 289–98.
[12] Ryu KH, Haile SM. Chemical stability and proton conductivity of doped $BaCeO_3$-$BaZrO_3$ solid solutions. Solid State Ionics 1999;125:355–67.
[13] Wang D, Yu RD, Feng SH, Zheng WJ, Takei T, Kumada N. Hydrothermal synthesis of perovskite-type solid solution of $(1-x)BaTiO_3 \cdot xLa_{2/3}TiO_3$. Solid State Ionics 2002;151:329–33.
[14] Babilo P, Uda T, Haile SM. Processing of yttrium-doped barium zirconate for high proton conductivity. J Mater Res 2007;22:1322–30.
[15] Cervera RB, Oyama Y, Yamaguchi S. Low temperature synthesis of nanocrystalline proton conducting $BaZr_{0.8}Y_{0.2}O_{3-\delta}$ by sol–gel method. Solid State Ionics 2007; 178:569–74.
[16] Gu HG, Ran R, Zhou W, Shao ZP. Anode-supported ScSZ-electrolyte SOFC with whole cell materials from combined EDTA–citrate complexing synthesis process. J Power Sources 2007;172:704–12.
[17] Guo YM, Lin Y, Ran R, Shao ZP. Zirconium doping effect on the performance of proton-conducting $BaZr_yCe_{0.8-y}Y_{0.2}O_{3-\delta}$ ($0.0 \leq y \leq 0.8$) for fuel cell applications. J Power Sources 2009; 193:400–7.
[18] Perry NH, Kim S, Mason TO. Local electrical and dielectric properties of nanocrystalline yttria-stabilized zirconia. J Mater Sci 2008;43:4684–92.
[19] Gemmen RS, Trembly JP. On the mechanisms and behavior of coal syngas transport and reaction within the anode of a solid oxide fuel cell. J Power Sources 2006;161:1084–95.
[20] Zhong ZM. Stability and conductivity study of the $BaCe_{0.9-x}Zr_xY_{0.1}O_{2.95}$ systems. Solid State Ionics 2007;178: 213–20.
[21] Gong M, Liu X, Trembly JP, Johnson C. Sulfur-tolerant anode materials for solid oxide fuel cell application. J Power Sources 2007;168:289–98.
[22] Fabbri E, D'Epifanio A, Bartolomeo ED, Licoccia S, Traversa E. Tailoring the chemical stability of $Ba(Ce_{0.8-x}Zr_x)Y_{0.2}O_{3-\delta}$ protonic conductors for intermediate temperature solid oxide fuel cells (IT-SOFCs). Solid State Ionics 2008;179: 558–64.
[23] Lu JD, Wang L, Fan LH, Li YH, Dai L, Guo HX. Chemical stability of doped $BaCeO_3$-$BaZrO_3$ solid solutions in different atmospheres. J Rare Earth 2008;26:505–10.
[24] Zeng Y, Mao PL, Jiang SP, Wu P, Zhang L, Wu P. Prediction of oxygen ion conduction from relative Coulomb electronic interactions in oxyapatites. J Power Sources 2011;196: 4524–32.
[25] Tu CS, Chien RR, Schmidt VH, Lee SC, Huang CC, Tsai CL. Thermal stability of $Ba(Zr_{0.8-x}Ce_xY_{0.2})O_{2.9}$ ceramics in carbon dioxide. J Appl Phys 2009;105:103504.
[26] Fuentes RO, Baker RT. Synthesis and properties of gadolinium-doped ceria solid solutions for IT-SOFC electrolytes. Int J Hydrogen Energy 2008;33:3480–4.
[27] Lv J, Wang L, Lei D, Guo H, Kumar RV. Sintering, chemical stability and electrical conductivity of the perovskite proton conductors $BaCe_{0.45}Zr_{0.45}M_{0.1}O_{3-\delta}$ (M = In, Y, Gd, Sm). J Alloys Compd 2009;467:376–82.
[28] Azad AK, Irvine JTS. Synthesis, chemical stability and proton conductivity of the perovksites $Ba(Ce, Zr)_{1-x}Sc_xO_{3-\delta}$. Solid State Ionics 2007;178:635–40.

[29] Xie K, Ma Q, Lin B, Jiang Y, Gao J, Liu X, et al. An ammonia fuelled SOFC with a $BaCe_{0.9}Nd_{0.1}O_{3-\delta}$ thin electrolyte prepared with a suspension spray. J Power Sources 2007;170:38–41.
[30] Chien RR, Tu CS, Schmidt VH, Lee SC, Huang CC. Synthesis and characterization of proton-conducting $Ba(Zr_{0.8-x}Ce_xY_{0.2})O_{2.9}$ ceramics. Solid State Ionics 2010;181:1251–67.
[31] Long RQ, Huang YP, Wan HL. Surface oxygen species over cerium oxide and their reactivities with methane and ethane by means of in situ confocal microprobe Raman spectroscopy. J Raman Spectrosc 1997;28:29–32.
[32] Kim BK, Hamaguchi HO. Mode assignments of the Raman spectrum of monoclinic zirconia by isotopic exchange technique. Phys Stat Sol B 1997;203:557–63.